Biomaterials 199 (2019) 63–75

Contents lists available at ScienceDirect

Biomaterials

journal homepage: www.elsevier.com/locate/biomaterials

Decellularised extracellular matrix-derived peptides from neural retina and retinal pigment epithelium enhance the expression of synaptic markers and light responsiveness of human pluripotent stem cell derived retinal organoids

Birthe Dorgau[a,1], Majed Felemban[a,1], Gerrit Hilgen[b], Martin Kiening[a], Darin Zerti[a], Nicola Claire Hunt[a], Mary Doherty[c], Phil Whitfield[c], Dean Hallam[a], Kathryn White[d], Yuchun Ding[e], Natalio Krasnogor[e], Jumana Al-Aama[f], Hani Z. Asfour[g], Evelyne Sernagor[b], Majlinda Lako[a,*]

[a] Institute of Genetic Medicine, Newcastle University, UK
[b] Institute of Neuroscience, Newcastle University, UK
[c] University of the Highlands and Islands, UK
[d] EM Research Services, Newcastle University, UK
[e] Interdisciplinary Computing and Complex Biosystems (ICOS) Research Group, Newcastle University, UK
[f] Department of Genetic Medicine and Princess Al-Jawhara Center of Excellence in Research of Hereditary Disorders, Faculty of Medicine, King Abdulaziz University, Saudi Arabia
[g] Department of Medical Microbiology and Parasitology, Faculty of Medicine, Princess Al-Jawhara Center of Excellence in Research o Hereditary Disorders, King Abdulaziz University, Jeddah, Saudi Arabia

HIGHLIGHTS

- Early/middle stages of differentiation are not affected by decel NR, decel RPE or CM RPE supplementation.
- Supplementation with decel RPE enhances RPE generation.
- CM RPE and decel RPE enhance the formation of rod photoreceptors.
- Decel RPE and decel NR enhance the expression of synaptic markers and the light driven responses.
- Retinal decellularised petides enhance the differentiation and functionality of hPSC-derived retinal organoids.

ARTICLE INFO

Keywords:
Decellularisation
Extracellular matrix
RPE
Neural retina
Retinal organoids
Human pluripotent stem cells

ABSTRACT

Tissue specific extracellular matrices (ECM) provide structural support and enable access to molecular signals and metabolites, which are essential for directing stem cell renewal and differentiation. To mimic this phenomenon *in vitro*, tissue decellularisation approaches have been developed, resulting in the generation of natural ECM scaffolds that have comparable physical and biochemical properties of the natural tissues and are currently gaining traction in tissue engineering and regenerative therapies due to the ease of standardised production, and constant availability. In this manuscript we report the successful generation of decellularised ECM-derived peptides from neural retina (decel NR) and retinal pigment epithelium (decel RPE), and their impact on differentiation of human pluripotent stem cells (hPSCs) to retinal organoids. We show that culture media supplementation with decel RPE and RPE-conditioned media (CM RPE) significantly increases the generation of rod photoreceptors, whilst addition of decel NR and decel RPE significantly enhances ribbon synapse marker expression and the light responsiveness of retinal organoids. Photoreceptor maturation, formation of correct synapses between retinal cells and recording of robust light responses from hPSC-derived retinal organoids remain unresolved challenges for the field of regenerative medicine. Enhanced rod photoreceptor differentiation, synaptogenesis and light response in response to addition of decellularised matrices from RPE and neural retina as

* Corresponding author. Newcastle University, Institute of Genetic Medicine, International Centre for Life, Central Parkway, Newcastle, NE1 3BZ, UK.
E-mail address: majlinda.lako@ncl.ac.uk (M. Lako).
[1] both authors contributed equally.

https://doi.org/10.1016/j.biomaterials.2019.01.028
Received 23 October 2018; Received in revised form 11 January 2019; Accepted 20 January 2019
Available online 22 January 2019

shown herein provide a novel and substantial advance in generation of retinal organoids for drug screening, tissue engineering and regenerative medicine.

1. Introduction

The potential of human pluripotent stem cells (hPSCs) to differentiate into retinal cells makes them a great tool for the study of inherited and age related retinal dystrophies, drug screening/repurposing and provision of a limitless source of cells for cell based therapies. In the last decade, seminal discoveries made by Sasai's group have led to the generation of retinal organoids containing key retinal cell types such as photoreceptors, Müller glia and other retinal neurons organized in a laminated structures, from murine, primate and human embryonic stem cells (hESCs) and human induced pluripotent stem cells (hiPSCs) [1–6]. Intense work has been performed by several groups worldwide to improve the robustness and efficiency of differentiation protocols and to understand the factors and signalling pathways that are required to enhance retinal specification. This has led to generation of multiple *in vitro* disease models for inherited and age related disease and increased availability of human retinal tissue for basic biology and proof-of-concept toxicology and transplantation studies [4,7,8]. However, current differentiation protocols are impeded by several key challenges as follows: *(1)* high intra line and inter experimental variability; (*2*) laborious and lengthy methods [9]; (*3*) inability to generate the correct proportions of all retinal cell types and to maintain the three clearly separated nuclear layers and appropriate synaptic connections in long term cultures [9]; (*4*) inability to elicit light responses which are fully comparable to adult retina [3,5,9–12] and (*5*) uncertainty about the extent to which hESCs- and hiPSCs-derived retinal organoids recapitulate *in vivo* human retinal development. Many groups have reported the generation of retinal pigment epithelium (RPE) cells [9,12–14], however the latter are often found at the opposite side of the retinal organoid (and not adjacent to neural retina (NR) as *in vivo)*), resulting in impaired interaction between the NR and RPE, affecting retinal lamination, spatial reorganisation and maturation of photoreceptors, all of which are dependent on the RPE-NR interactions [15,16].

In vivo, RPE cells release many extracellular molecules (ECMs) (for example laminin, collagen and hyaluronic acid) which help to maintain retinal integrity and photoreceptor viability and function [17–19]. Indeed, *in vitro* proteomic studies have shown the secretion of numerous trophic factors and ECMs molecules, including fibronectin, collagen and laminin from foetal and adult RPE into the culture media [20]. The biological effect of the RPE secreted factors is reflected in enhanced proliferation, neurite outgrowth and differentiation of the photoreceptors isolated from neonatal rat retina co-cultured with RPE conditioned media (CM RPE) [21] as well as enhanced RPE differentiation from hESCs [22]. Co-culture of NR with CM RPE significantly decreased the thinning of outer nuclear layer, photoreceptor axon retraction and apoptosis [23], thus suggesting the presence of key factors in CM RPE which support photoreceptor viability under *in vitro* culture conditions. Co-culturing of rat NR with RPE cells also has been shown to promote the attachment of the photoreceptors, axons growth and migration of their cell bodies toward the RPE cells *in vivo* as well as photoreceptors development by increasing the synthesis of rhodopsin [16]. Given the close interactions of RPE with NR, their co-culture has been used to support the maintenance of NR in novel organotypic culture model [24]. For example, Kaempf et al. indicated that co-culture of adult porcine NR with choroid-RPE explant *in vitro* enhanced the maintenance of the retina by reducing apoptosis in both nuclear cell layers, decreasing gliosis and increasing glutamate synthetase compared to retina cultured alone [24].

In addition to secreted factors provided in CM and direct co-culture of several cell types, tissue decellularisation has been proposed as a useful method for providing the necessary biochemical and biophysical features of cellular niches that are needed to promote progenitor and stem cell differentiation and engraftment [25–32]. Tissue decellularisation consists of removing the cellular material from tissues so that only the ECM components remain [25]. This process preserves the integrity of the ECM which can be used as an additional culture medium supplement, as a scaffold to support cell engraftment and differentiation and a source of biochemical and biophysical cues for the cells that reside within it [25]. To date, decellularised ECM (decel ECM) has been successfully achieved from many tissues including heart, liver, lung, kidney and brain [26–34]. Several groups have also performed decellularisation of tissues in the eye including cornea, retina, Bruch's membrane and RPE [25,35–39]. More recently, decel ECM has been prepared from bovine NR and shown to support the attachment and differentiation of human retinal progenitor cells *in vitro* [36]. Despite these encouraging findings, the role of decellularised ECM from neural retina or RPE on the generation and functionality of hESC- and hiPSC-derived retinal organoids has not been addressed to-date. In this study we report the successful derivation of decellularised ECM from adult bovine NR (decel NR) and RPE (decel RPE) and show a significant role in enhancing photoreceptor differentiation, synaptogenesis and light responsiveness of pluripotent stem cell derived retinal organoids.

2. Materials and methods

2.1. Preparation of RPE conditioned medium (CM RPE)

CM RPE was collected every day from polarized mature RPE (TER > 250Ω) derived from hESCs and hiPSCs cultured in DMEM:F12 medium (Life Technologies, UK) supplemented with 2% B27 (Gibco, UK) & 1% N2 (Gibco, UK), based on a protocol published by our group [40,41]. The RPE cells density was 100,000 cells/cm^2. CM RPE was collected and combined from both hESC- and hiPSC-derived RPE then centrifuged at 1000 rpm for 4 min, diluted 1:3.5 in retinal organoid media and filtered prior to usage.

2.2. Preparation of decellularised ECM from NR and RPE

RPE & NR were isolated from four adult bovine eyes freshly collected from the abattoir within 1 h after slaughter. The eyeballs were hemisected to remove the cornea and vitreous humour and the retina was peeled very gently from the RPE and immersed into phosphate buffer saline (PBS, Sigma-Aldrich, UK). The isolated tissues (RPE/NR) were washed twice with PBS on orbital shaker at 60 rpm for 5 min. The RPE and NR decellularisation procedures were performed following the protocol published by Medberry et al., 2013 [42]. In brief, the RPE was washed as follow: distilled H_2O (16 h at 4 °C, 60 rpm); 0.02% trypsin/0.05% EDTA (60 min at 37 °C, 20 rpm); 3% TritonX-100 (60 min at 4 °C), 1.0 M Sucrose (15 min at 4 °C), distilled H2O (15 min), 4% Sodium Deoxycholate (60 min at 4 °C), 0.1% peracetic acid in 4% Ethanol (V/V) (120 min at 4 °C), PBS (15 min at 4 °C), distilled H_2O (15 min at 4 °C) twice. Each step was performed under 60 rpm stirring unless otherwise stated and followed by distilled water rinsing through a strainer. Retinae were processed following the same stages under milder conditions: concentrations, incubation times and stirring rates all underwent a two-fold decrease besides Trypsin/EDTA (0.005%/0.0125%, 30 min at 37 °C, 20 rpm) and Sucrose (0.1 M, 30 min at 4 °C). Decellularised RPE and NR were snap-frozen in liquid nitrogen for 1–2 min before freeze-drying at −54 °C, 0.5 bar for 48 h (FreeZone

Labconco, Chemical Engineering Department, Newcastle University). The dried decellularised RPE and NR were then stored at −20 °C until digestion. The tissues were snap-frozen in liquid nitrogen for 30–60 s, and immediately crushed with a glass pestle in a mortar previously cooled on dry-ice to obtain a fine powder. 10 mg of each powder was digested by 1 mg/ml pepsin (porcine gastric mucosa ≥2500 unit/mg, Sigma-Aldrich, P7012) in 0.01 N HCl. The solutions were centrifuged at 4000 rpm for 15 min, filtered on a 40 μm strainer and stored at −20 °C until needed.

2.3. ECMs and DNA quantification

The following colorimetric assays were performed to quantify the amount of collagen, glycosaminoglycan (GAGs), Hyaluronic Acid, Laminin and DNA content in the decel RPE and decel NR, native RPE and NR, CM RPE the RPE media.

2.3.1. Hydroxyproline assay

Hydroxyproline assay kit (BioVision, K555-100) was used according to manufacturer's protocol to quantify the amount of collagen. The absorbance was measured at 560 nm in a plate reader (Varioskan LUX, Thermo Fisher Scientific, UK). Each sample was run in triplicate and the average absorbance value was calculated. The background value was corrected against the blank controls and the concentration of each sample was determined against a Hydroxyproline standard.

2.3.2. Dimethylmethylene blue assay (DMMB)

Sulphated GAGs concentration was measured using dimethylmethylene blue assay (DMMB) which results in a change in the absorbance spectrum while forming the GAG-DMMB complex. The DMMB reagent was prepared as follows: 16 mg DMMB in 1 L double-distilled water containing 3.04 g glycine, 1.6 g NaCl and 95 ml of 0.1 M Acetic Acid. The pH of the solution was 3.0 and all the DMMB components were from (Sigma-Aldrich, UK). 20 μl of each sample was transferred to a 96-well plate and incubated with DMMB reagent (200μl/sample) for 5 s. Then, the absorbance value was read at 525 nm using Varioskan LUX plate reader. The average value was calculated, corrected against a blank control and the concentration was determined against a standard chondroitin 4-sulfate from bovine (Sigma-Aldrich, UK).

2.3.3. Turbidimetric measurement of hyaluronic acid

Hyaluronic Acid was quantified using a turbidimetric protocol, based on the formation of insoluble complex between Cetyltrimethylammonium bromide (CTAB; Sigma-Aldrich, UK) and the isolated acid mucopolysaccharides [43]. The samples were diluted (1:1 ratio) in acetate buffer (0.2 M Acetic acid, 0.15 M NaCl, pH 6.0). Then, 100 μl of the solution (triplicate/sample) was transferred to a 96-well plate and incubated at 37.5 °C for 15 min. Afterwards, 200 μl of CTAB reagent (2.5 g of CTAB dissolved in 100 ml of 2% NaOH) was added per well and the plate was incubated at room temperature on a plate shaker (300 rpm) for 30 s before the absorbance was measured at 405 nm using Varioskan LUX plate reader. The mean absorbance value was calculated and corrected against the blank control. Then, the concentration of Hyaluronic Acid was determined against a standard Hyaluronic Acid sodium salt from *Streptococcus equi* (Sigma-Aldrich, UK).

2.3.4. Laminin

A bovine Laminin enzyme-linked immunosorbent assay (Laminin-ELISA) kit (Amsbio, UK) was used according to the manufacturer's protocol to quantify Laminin concentration in the native and decellularised RPE and NR. The absorbance was measured at 450 nm using a Varioskan LUX plate reader. The mean absorbance value was calculated and the concentration of Laminin was determined against a Laminin standard. Since CM RPE was collected from human RPE cells, Laminin quantification in normal and CM RPE was performed on a different ELISA kit from human (Aviva Systems Biology, UK) following the manufacturer's protocol. The absorbance was measured as described above.

2.3.5. DNA quantification

The cellular DNA content was measured using a Hoechst fluorometric assay following a protocol indicated by Rago et al., 1990 [44]. The samples were diluted (1:1 ratio) in TNE buffer (10 mM Tris, 2 M NaCl, 1 mM EDTA, pH 7.4) containing 20 μg/ml of Hoechst 33258 (Life Technologies, UK). Then, 200 μl of the solution (triplicate/sample) was transferred to a 96-well plate. The fluorescence intensity was proportional to the amount of DNA in the sample and was measured at a fluoro-chrome excited at 350 nm and the emission wavelength was read at 460 nm using Varioskan LUX plate reader. Then, the concentration was determined against a DNA standard from calf thymus (Sigma-Aldrich, UK).

2.4. Peptide analysis by high-resolution mass spectrometry

Samples were subjected to acetone precipitation, with the acetone fraction, containing peptides, dried under vacuum and reconstituted in 0.1% formic acid. Peptide analysis was performed in positive ion mode using a Thermo LTQ-Orbitrap XL LC-MS^n mass spectrometer equipped with a nanospray source and coupled to a Waters nanoAcquity UPLC system. The samples were initially desalted and concentrated on a BEH C18 trapping column (Waters, Manchester, UK). The peptides were then separated on a BEH C18 nanocolumn (1.7 μm, 75 μm × 250 mm, Waters) at a flow rate of 300 nL/min using an ACN/water gradient; 1% ACN for 1 min, followed by 0–62.5% ACN over 21 min, 62.5–85% ACN for 1.5 min, 85% ACN for 2 min and 1% ACN for 15 min. MS spectra were collected using data-dependent acquisition in the range m/z 200–2000 using a precursor ion resolution of 30,000 following which individual precursor ions (top 5) were automatically fragmented using collision induced dissociation (CID) with a relative collision energy of 35%. Dynamic exclusion was enabled with a repeat count of 2, repeat duration of 30 s and exclusion duration of 180 s. Data were first analysed using Proteome Discoverer v1.1 (Thermo) with the MASCOT (Matrix Science, London, UK) search engine against the UniProt database. The initial search parameters allowed for oxidation of methionine, a precursor mass tolerance of 10 ppm, a fragment mass tolerance of ± 0.5 Da, and a FDR of 0.01. For relative quantification, raw data files were analysed using Progenesis QIP (Non-Linear Dynamics, Newcastle, UK) using the search parameters outlined above.

2.5. Human pluripotent stem cells differentiation to retinal organoids

Retinal organoids were derived from two different cell lines: hiPSCs derived from adult fibroblasts (SB-Ad3) [45] and hESCs (H9, Wicell Inc.). Stem cells were expanded in mTeSR™1 (StemCell Technologies, 05850) at 37 °C and 5% CO_2 on 6 well plates pre-coated with Low Growth Factor Matrigel (Corning, 354230). The retinal organoids were generated following a protocol described in Mellough et al., 2015 [46] with the addition of ROCK inhibitor (Y-27632 dihydrochloride) (10 μM) for the first 48 h of differentiation. Further modifications included the addition of 10% Fetal Calf Serum (Life Technologies, UK), T3 (40 ng/ml; Sigma-Aldrich UK), Taurine (0.1 mM; Sigma-Aldrich UK) and Retinoic Acid (0.5 μM; Sigma-Aldrich UK) from day 18 of differentiation onwards [47, 53]. After day 18 of differentiation, the cells were divided into 4 groups with different cultural conditions: Control, CM RPE, decel NR (10 μg/ml) and decel RPE (10 μg/ml) (Fig. S1). Retinal organoids were collected on day 35, 90 and 150 for qRT-PCR and immunohistochemistry (IHC). For IHC the organoids were fixed in 4% (w/v) PFA for 20 min, followed by three washes in PBS and overnight cryoprotection in 30% sucrose in PBS before embedding in OCT medium (Cell Path Ltd., Newtown, UK). 10 μm cryostat sections were collected using a Leica Cm1860 cryostat (Leica, Germany). For qRT-

PCR retinal organoids were collected, washed with PBS and immediately frozen at −80 °C.

2.6. Immunohistochemistry

Cryosections were air-dried, washed several times in PBS and incubated in blocking solution (10% normal goat serum, 0.3% Triton-X-100 in PBS) for 1 h at room temperature. Antibody diluent solution was prepared (1% bovine serum albumin (BSA), 0.3% Triton–X100 in PBS) and used to dilute all antibodies. Tissue sections were incubated with widely used retinal cell type specific primary antibodies (Table S1) overnight at 4 °C and washed several times with antibody diluent before incubating with secondary antibodies (Table S1) at room temperature for 2 h. Afterwards, sections were washed three times in PBS and mounted with Vectashield (Vector Laboratories, Burlingame, CA) containing Hoechst (Life Technologies, UK). To assess the specificity of primary antibody binding, these were omitted and replaced with isotype controls as described in our recent publication [47]. For all antibodies, no non-specific binding was observed [47]. To assess the specificity of secondary antibody staining, primary antibodies were omitted. Again no non-specific binding was observed (Fig. S2).

2.7. Image capture and analysis

Images were captured using an Axio Imager upright microscope with Apotome structured illumination fluorescence (Zeiss, Germany) using 20x objective and 63x oil objective operated with AxioVision software. Tissue sections of three biological replicates of hPSCs-derived retinal organoids were analysed. Each biological replicate of day 35, 90 and 150 retinal organoids included 10–15 organoids per condition. Final images are presented as a maximum projection and adjusted for brightness and contrast in Adobe Photoshop (Adobe Systems).

2.7.1. Image quantification

Cell image quantitation was performed using the MATLAB software (Mathworks, MA). The data was presented as image segmentation using Hysteresis thresholding technique to segment the cells and filter out any noise background from the images [48]. The measuring property of MATLAB (regionprops) was used to represent all the pixels of each image as single region in order to extract the information about each cell including the size, average intensity value and length. After obtaining the final segmentation information, the total size and the percentage of the positive cells were calculated and exported as excel file for further analysis.

The quantification of synaptic marker proteins, Bassoon and CtBP2, was performed using ImageJ (NIH, Bethesda, MD). For hESCs and hiPSCs, 5–7 and 3 individual organoids per condition were analysed respectively. All images were taken with the same exposure time and three squares (500 × 500 pixels) to cover the whole retinal structure were validated in each organoid image. Number of patches and median intensity were calculated automatically by ImageJ using an intensity threshold [49] to ensure an accurate count with same conditions for all groups. All results were further analysed using Microsoft Excel and Prism (GraphPad, USA).

2.8. qRT-PCR

15-20 retinal organoids were homogenised using a Dounce Tissue Grinder (Sigma-Aldrich, UK) to extract the RNA using the Promega tissue extraction kit (Promega, USA) as per the manufactures instructions. 1 μg of RNA was reverse transcribed using random primers (Promega, USA). qRT-PCR was performed using a Quant Studio 7 Flex system (Applied Biosystems, USA) with SYBR Green reaction mixture (Promega, USA). Each primer (Table S2) was used at a concentration of 1 μM, and at a ratio of 50:50 for forward and reverse. The reaction parameters were as follows: 95 °C for 15 min to denature the cDNA and primers, 40 cycles of 94 °C for 15 s followed by primer specific annealing temperature for 30 s (60 °C), succeeded by a melt curve. A comparative cycle threshold (Ct) method was used to calculate the levels of relative expression, whereby the Ct was normalised to the endogenous control (*GAPDH*). This calculation gives the Δ^{Ct} value, which was then normalised to a reference sample (i.e. control group), giving the $\Delta\Delta^{Ct}$. The fold change was calculated using the following formula: $2\text{-}\Delta\Delta^{Ct}$.

2.9. Electrophysiological recordings

24 h prior to electrophysiological recordings, 9-cis retinal (10 nM; Sigma-Aldrich, UK) was added to the incubation medium. Organoids were transferred to 34 °C artificial cerebrospinal fluid (aCSF) containing the following (in mM): 118 NaCl, 25 $NaHCO_3$, 1 NaH_2PO_4, 3 KCl, 1 $MgCl_2$, 2 $CaCl_2$, 10 glucose, 0.5 L-Glutamine and 0.01 9-cis-retinal. Organoids were opened longitudinally and placed, with the presumed retinal ganglion cell (RGC) layer facing down on the electrodes, onto a 4096 channel multielectrode array (MEA), flattened with a translucent polyester membrane filter (Sterlitech Corp., Kent, WA, USA). The organoids were allowed to settle for at least 2 h. Recordings were performed on the BioCam4096 MEA platform with BioChips 4096S+ (3Brain GmbH, Lanquart, Switzerland), integrating 4096 square microelectrodes in a 64 × 64 array configuration.

Light stimuli were projected as described previously [50]. Broad white (high photopic) light pulses (WLP, 200 ms, 217 μW/cm2 irradiance, 1 Hz) were flashed for 5 min onto the organoids following recording spontaneous activity in the dark for 5 min. The drug cGMP (8-Bromoguanosine 3′, 5′-cyclic monophosphate, Sigma-Aldrich, MO) was puffed in the recording chamber (final concentration: 100 μM) and activity was recorded continuously for 4 min, starting at 2 min before the puff.

To reliably extract spikes from the raw traces, a quantile based event detection was used [51]. Single-unit spikes were sorted using an automated spike sorting method for dense, large-scale recordings [52]. Statistical significance (unpaired t-test) and firing rate analyses were evaluated by using MATLAB (Mathworks, MA) and Prism (GraphPad, CA). RGCs were considered responsive if they show at least 25% increase or decrease in spiking activity during 30 s after WLP onset compared to a similar time window before the light was turned on. For each cell, all spikes occurring during these two time windows were counted and the mean % change (± SEM) in activity between windows was calculated.

2.10. Transmission electron microscopy (TEM)

Cells were fixed with 2% glutaraldehyde and kept at 4 °C. Sample processing and TEM was performed at Newcastle University Electron Microscopy Research Services. Ultrathin sections were stained with heavy metal salts (uranyl acetate and lead citrate) and imaged on a Philips CM100 TEM (Philips, Japan).

2.11. Statistical analyses

All statistical tests were performed using Prism (GraphPad, USA). The standard errors of all means (SEM) were calculated. Statistical significance was tested using one-way ANOVA (Dunnett statistical hypothesis for multiple test correction). Asterisk = p-value < 0.05, two asterisks = P-value < 0.01, three asterisks = P-value < 0.001, four asterisks = P-value < 0.0001.

3. Results

3.1. ECMs composition in CM RPE, decel NR & decel RPE

In order to examine the role of decellularised ECM on the

differentiation and functionality of hPSCs–derived retinal organoids, NR and RPE tissue were extracted and decellularised from adult bovine eyes [42]. To confirm the efficiency of the decellularisation process, the DNA content was assessed in decel NR and RPE samples. These results indicated the DNA content to be 8.5 and 4.3 μg/mg of initial dry weight of NR and RPE, respectively (Fig. S3A), which was significantly lower than the amount of DNA in the native tissues, indicating that the bulk of cellular material was removed after the decellularisation process from the native retina (~92%) and RPE (~80.5%). This result was similar to that reported by Kundu et al., 2016 where (~94%) of cellular material was removed after the decellularisation of NR from bovine eyes [36].

The CM was collected from polarized RPE cells derived from hPSCs and the key ECM components (collagen, Laminin, GAGs and HA) were quantified and compared to RPE media and native tissue of bovine retina and RPE, respectively (Figs. S3B–D and Table S3). The concentration of all analysed ECM components (collagen, Laminin, GAGs and HA) was significantly increased in the CM RPE compared to the normal RPE media (Fig. S3B and Table S3). Opposite results were found for the native retina after decellularisation, revealing a significant decrease in GAGs and HA in the decel NR compared to the native retina (Fig. S3C and Table S3). Similar to decel NR, the collagen, GAGs and HA were significantly reduced in the decel RPE compared to the native RPE after decellularisation (Fig. S3D and Table S3). Together these results indicate that some of the ECM components (collagen, sulphated GAGs and HA) were lost during the decellularisation procedures; however laminin concentration was not affected by this process (Figs. S3C and D).

Proteomics analysis of decel NR and RPE was carried out to gain more insights into the peptides present in these samples (Table S4 and Table S5). A large number of ECM components including various collagen and laminin chains as well as versican were identified in both decel NR and RPE. A comparative analysis indicated significant differences in the abundance of collagen chains between decel RPE and decel NR (Table S6). Versican was more abundant in decel NR, whilst laminin chains showed no significant difference in expression between the two samples.

3.2. *Effects of ECM supplementation on early and middle stages of retinal differentiation*

The effects of each ECM supplementation (CM RPE, decel NR or decel RPE) in retinal organoids was analysed in detail using qRT-PCR

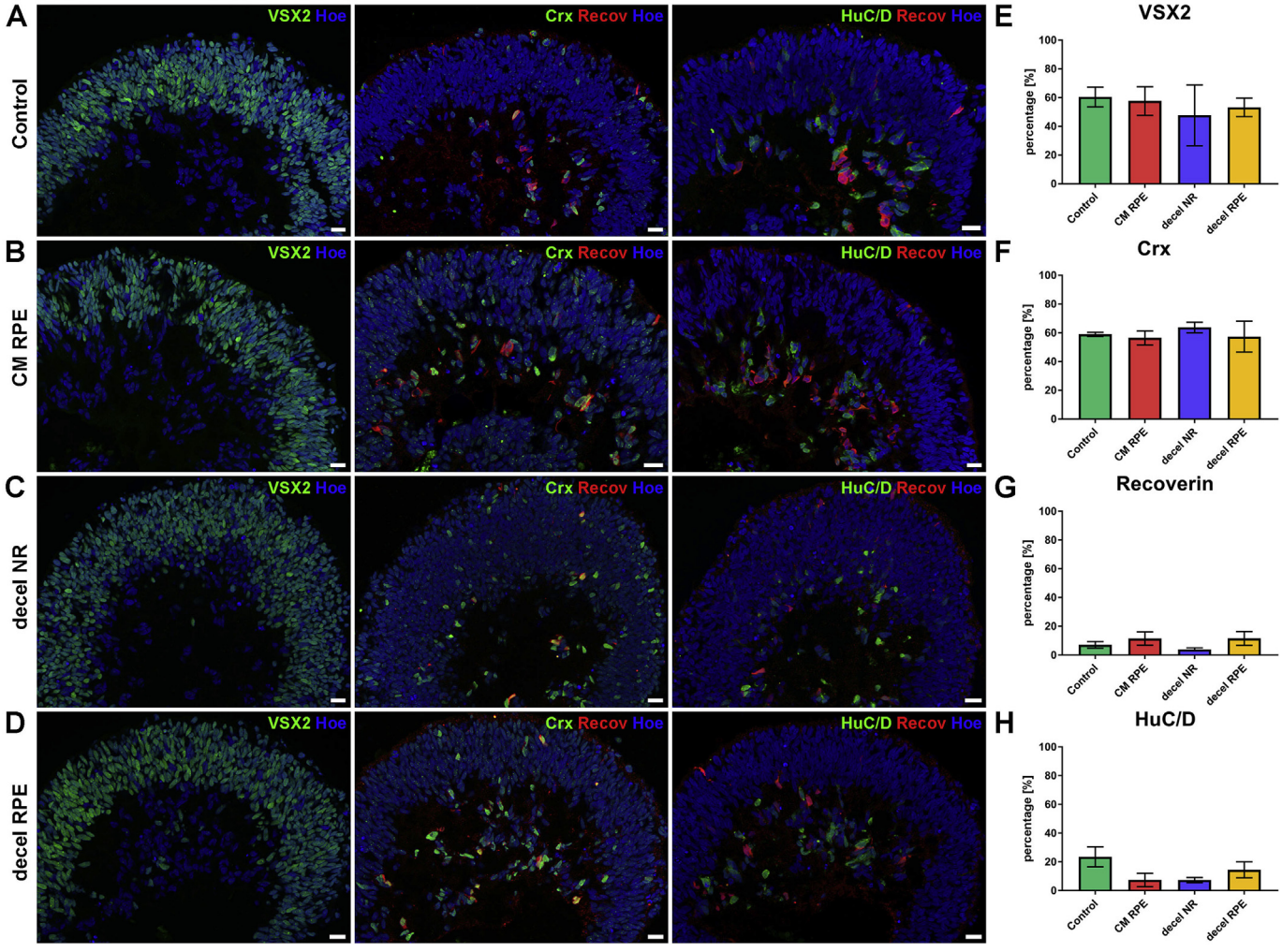

Fig. 1. hESCs-derived retinal organoid characterisation at day 35 of differentiation in all four culture conditions. (A–D) Expression of retinal progenitor cells (VSX2, green), photoreceptors (Crx, green; Recoverin, red) and amacrine/ganglion cells (HuC/D, green) in control (A), CM RPE (B), decel NR (C) and decel RPE (D) condition, showing a thick apical layer of retinal progenitor cells and some photoreceptors across the whole organoid whereas most ganglion/amacrine cells were found in the centre of organoids. Nuclei are counterstained with Hoechst. Abbreviations: Hoe, Hoechst; Recov, Recoverin. Stars indicate background staining. Scale bars = 20 μm.(E–H) Cell quantification graphs of VSX2 (E), Crx (F), Recoverin (G) and HuC/D (H), revealing no significant differences between the control (green) and CM RPE (red), decel NR (blue) or decel RPE (yellow) conditions. Data is shown as mean ± SEM, n = 6–8 experiments performed in hESCs & hiPSCs. (For interpretation of the references to color in this figure legend, the reader is referred to the Web version of this article.)

and IHC with specific developmental marker proteins at different time points during differentiation. In addition, cell quantification analysis of key retinal markers was used to validate the impact of each ECM supplementation at key stages during the differentiation process (early: day 35, mid: day 90 and late: day 150). The stage selection for differentiation time course was based on our immunohistochemical characterisation of retinal organoids (already published by our group in Refs. [47,53]). This analysis has shown that day 35 (early stage) is characterised by the presence of an apical layer packed with VSX2 progenitors and a basal layer where the putative ganglion/amacrine HuC/D positive cells reside. The middle stage of differentiation (day 90) is characterised by the presence of RPE, photoreceptor precursors, RGCs and Müller glia cells, whilst day 150 is characterised by the presence of all key retinal cell types including photoreceptors, amacrine, bipolar and horizontal cells, as well as RGCs and Müller glia cells.

A thick layer of retinal progenitor cells, expressing VSX2, on the apical edge of retinal organoids derived from hESCs (Fig. 1A–D) and hiPSCs (Fig. S4) was observed in all conditions at day 35 of differentiation. Recoverin-positive photoreceptors and HuC/D-positive amacrine/ganglion cells were found in the centre of retinal organoids in all conditions (Fig. 1A–D and Fig. S4). The presence of ganglion cells (mostly in the centre of organoids) was confirmed by immunostaining with the retinal ganglion cell marker, RBPMS (Fig. S5). Crx, a marker for post-mitotic photoreceptors, was found across the entire neural retina, showing some positive cells in the centre as well as at the apical edge of organoids, where retinal progenitor cells are located (Fig. 1A–D and Fig. S4). Cell quantifications of retinal progenitor cells (VSX2), photoreceptor precursors (Crx and Recoverin), amacrine/ganglion cells (HuC/D) and ganglion cells (RBPMS) revealed no significant differences between all conditions (Fig. 1E–H and Fig. S5). This is in line with morphological observations, which showed a similar percentage of organoids had developed neural retina (with or without RPE) across different conditions at day 35 of differentiation (Fig. S6).

In comparison to day 35, a significant increase in retinal organoid growth was observed (Fig. S7) at day 90. At the same time the percentage of retinal organoids containing neural retinal structures with or without RPE (Figs. S6B and D) also increased at this timepoint. There were no significant differences between all groups, except for decel RPE condition of hESCs, which promoted formation of NR with RPE organoids ($p < 0.01$) compared to the control conditions (Fig. S6B). A thick layer of retinal progenitor cells was found in all conditions at day 90 of differentiation with a striking increase in the number of photoreceptors and amacrine/ganglion cells compared to day 35 of differentiation in both cell lines and all conditions (Fig. 2A–D and Fig. S8). The majority of HuC/D-positive amacrine and ganglion cells and RBPMS-positive ganglion cells were observed in the centre of organoids rather than across the neural retina (Fig. 2A–D and Fig. S5). A thin layer of photoreceptors, co-expressing Crx and Recoverin, was found at the apical edge of organoids; however Crx and Recoverin photoreceptor precursors were also found across the organoids as well as their basal side (Fig. 2A–D, Fig. S8A–D). NRL and RXRγ, which mark the post-mitotic rod and cone precursors respectively, were expressed at day 90 of

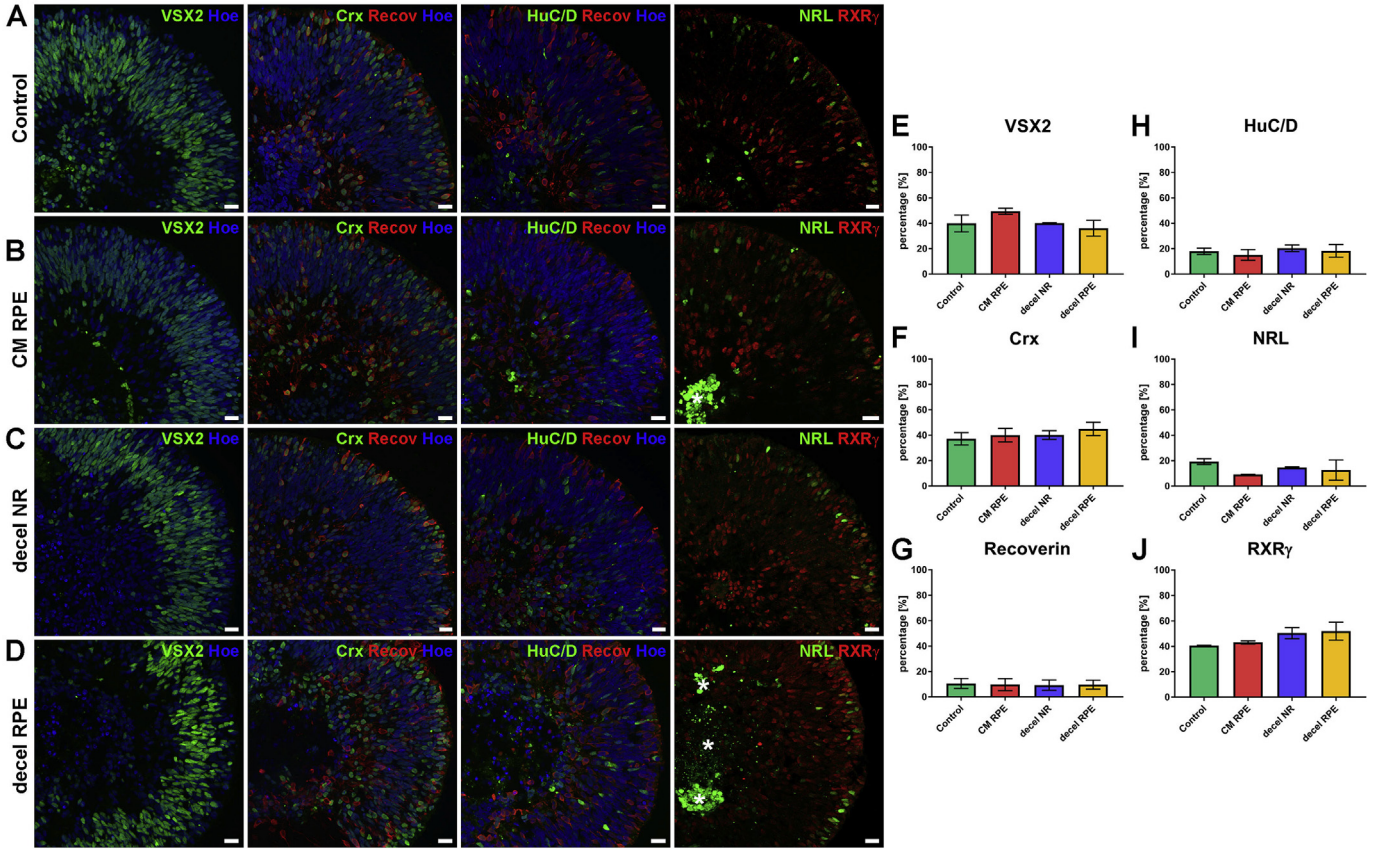

Fig. 2. hESCs-derived retinal organoid characterisation at day 90 of differentiation in all four culture conditions. (A–D) Expression of retinal progenitor cells (VSX2, green), photoreceptors (Crx, green; Recoverin, red), amacrine/ganglion cells (HuC/D, green), rod precursors (NRL, green) and cone precursors (RXRγ, red) in control (A), CM RPE (B), decel NR (C) and decel RPE (D) condition, showing a thick apical layer of retinal progenitor cells, photoreceptors in the apical and central sides of organoids and some rod precursor cells apically. Ganglion/amacrine cells and cone precursor cells are distributed throughout the whole organoid. Nuclei are counterstained with Hoechst. Abbreviations: Hoe, Hoechst; Recov, Recoverin. Scale bars = 20 μm. (E–J) Cell quantification graphs of VSX2 (E), Crx (F), Recoverin (G), HuC/D (H), NRL (I) and RXRγ (J), revealing no significant differences between the control (green) and CM RPE (red), decel NR (blue) or decel RPE (yellow) conditions. Data is shown as mean ± SEM, n = 6–8 experiments performed in hESCs & hiPSCs. (For interpretation of the references to color in this figure legend, the reader is referred to the Web version of this article.)

differentiation with slightly different distribution pattern. NRL-positive cells were mainly restricted to the apical edge of organoids whereas RXRγ-expressing cells were found across the neural retina in all conditions (Fig. 2A–D and Fig. S8A–D). In addition, there were fewer NRL-expressing cells compared to RXRγ cone precursors, as shown by the cell quantification analysis (Fig. 2I and J). No differences in retinal progenitor cells (VSX2), amacrine/ganglion cells (HuC/D), ganglion cells (RBPMS), photoreceptors (Crx and Recoverin) and rod and cone precursor marker (NRL and RXRγ) were found between all conditions by the cell quantification analysis (Fig. 2E–J and Fig. S5). Proliferating cells, detected by the marker protein Ki67 (Fig. S9) and apoptotic Caspase 3-positive cells (Fig. S10) were seen throughout retinal organoids, revealing no significant differences between culture conditions, except for Ki67 expression at day 35 (control vs decel RPE condition; Fig. S9). In summary, these data indicate that supplementation of culture media with CM RPE, decel NR and decel RPE does not affect retinal development at early and middle stages of differentiation.

3.3. ECM supplementation improves retinal differentiation at later stages

To assess the impact of ECM supplementation and presence of multiple retinal cell types during the later stages of differentiation, a large number of specific marker proteins were used for IHC analyses and TEM was performed for all conditions. Cell quantification analyses and qRT-PCR were also carried out to examine any differences between conditions.

At later stages of retinal differentiation (day 150) the percentage of organoids containing retinal bright phase neuroepithelium at the apical edge, increased slightly in both cell lines and all conditions compared to day 90 of differentiation (Fig. S6B and D). A remarkable increase of NR

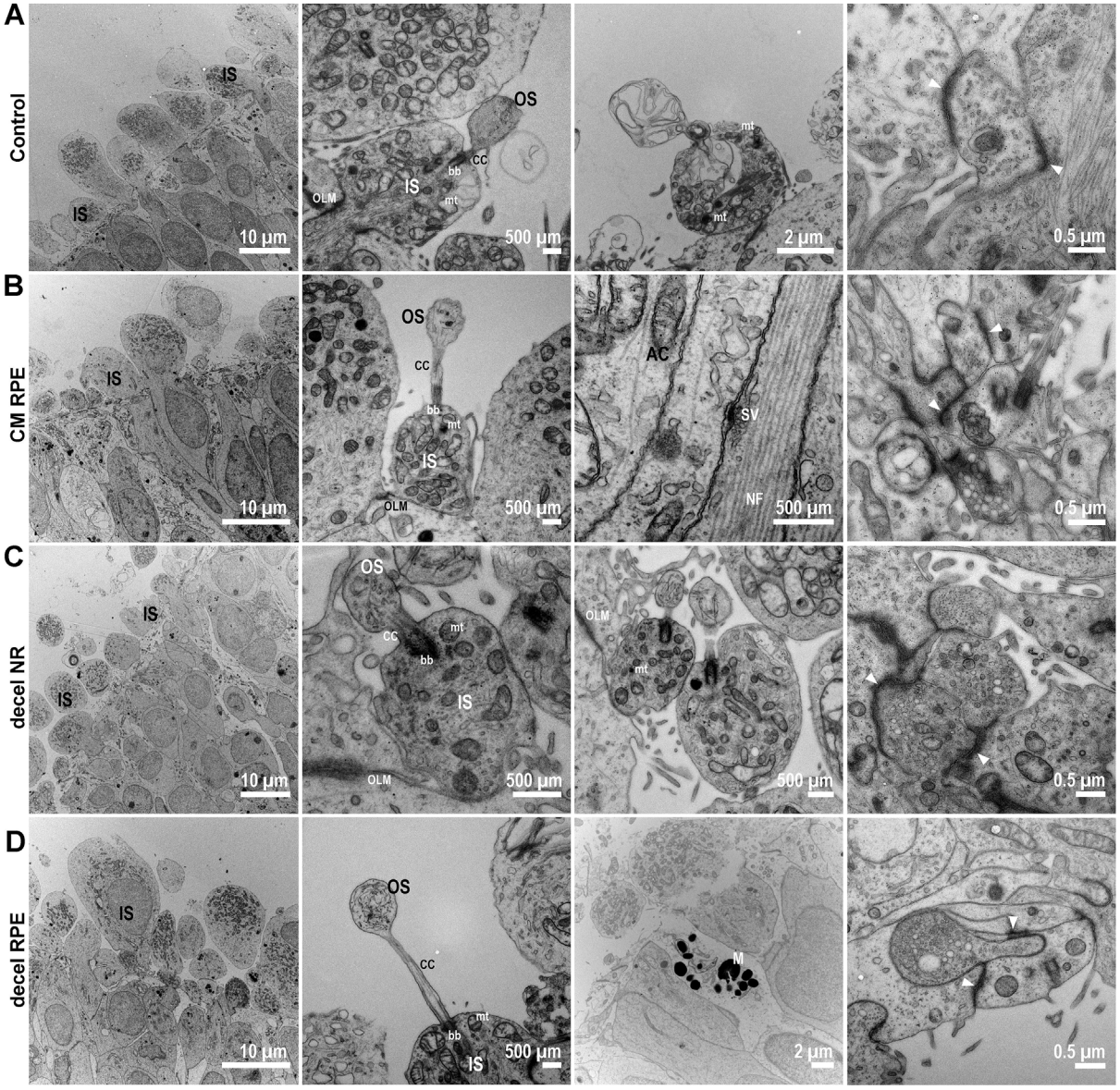

Fig. 3. Transmission electron microscopy analysis of hESCs-derived retinal organoids in all culture conditions. Ultrastructural analysis revealed photoreceptors containing inner (IS) and outer (OS) segments, connecting cilium (cc), basal body (bb) and an outer limiting membrane (OLM) underneath putative photoreceptor IS in control (A), CM RPE (B), decel NR (C) and decel RPE (D) condition. Other cell types including amacrine and Müller cells identified by the formation of neurofilaments were shown exemplary in CM RPE condition (B). Synaptic contacts (arrowheads) were found in all culture conditions (A–D). Melanosomes located in the apical part of organoids are shown in the "decel RPE" condition (D). Scale bars: 500 µm, 10 µm, 2 µm or 0.5 µm. Abbreviations: AC: amacrine cells; bb: basal body; cc: connecting cilium; IS: photoreceptor inner segments; mt: mitochondria; M: melanosomes; NF: neurofilaments; OLM: outer limiting membrane; OS: photoreceptors outer segments; SV: synaptic vesicles.

with RPE was seen in all conditions for hESCs in contrast to early stages of differentiation (Fig. S6B). Furthermore, there were significantly more NR with RPE organoids ($p < 0.05$) in decel RPE condition compared to control condition (Fig. S6B). The development of mature RPE cells was confirmed by TEM, showing more polarized melanosomes in decel RPE retinal organoids (Fig. 3D) compared to the control condition.

IHC analysis revealed a thick layer of photoreceptors, detected by Crx and Recoverin, on the apical side of retinal organoids in all conditions (Fig. 4 and Fig. S11), indicating the formation of an outer like nuclear layer (ONL). In all conditions higher magnifications of Recoverin-positive cells displayed characteristic morphological features of photoreceptors, including the connecting cilium, exemplified by ARL13B immunostaining, and developing outer segments (OS) as demonstrated by Gαt1 immunoreactivity (Fig. 4 and Fig. S11). These findings were confirmed by TEM, revealing the presence of organized photoreceptor-like ultra-structures features including the photoreceptor OS, inner segment (IS), connecting cilium and basal body in all conditions (Fig. 3). In addition, an outer limiting membrane (OLM) was observed basal to the IS of developing mitochondria-rich photoreceptors in all conditions (Fig. 3). Quantitative qRT-PCR analysis did not show any difference in the expression of *Crx* and *Recoverin,* moreover the number of Crx- and Recoverin-positive photoreceptors did not differ between conditions (Fig. S12). IHC analysis indicated that both photoreceptor types were found in all conditions in retinal organoids at day 150 of differentiation (Fig. 4 and Fig. S11). Rods, detected by Rhodopsin, were evenly distributed across the developing ONL of organoids (Fig. 4 and Fig. S11) with higher magnifications indicating typical rod morphology. Cell quantification analyses indicated a significant increase in the percentage of rods in CM RPE and decel RPE conditions when compared to control condition (Fig. S12B). These changes were confirmed by qRT-PCR results, showing higher expression of *RHO* in the CM RPE and decel RPE conditions (Fig. S12A). This suggested that the supplementation of CM RPE and decel RPE enhanced the development of rods. In contrast to rod expression, the expression of long/middle wavelength (OPN1LW/MW) and short wavelength (OPN1SW) cones was more sporadic within retinal organoids (Fig. 4 and Fig. S11), suggesting the beginning of opsin expression at this developmental stage. Nevertheless, both OPN1LW/MW and OPN1SW immunoreactive-positive cells were found at both the apical and basal side of retinal organoids and higher magnifications of both cone types display the typical cone morphology at this stage of differentiation (Fig. 4 and Fig. S11).

All other retinal cell-types (bipolar, horizontal, amacrine, ganglion and Müller cells) were found at day 150 of differentiation in retinal organoids derived from both cell lines and in all conditions (Fig. 5 and Fig. S11). HuC/D-positive amacrine/ganglion cells were mostly located in the centre of retinal organoids (Fig. 5 and Fig. S11). This was observed in all conditions (Fig. 5 and Fig. S11) without any difference in the percentage of HuC/D-positive cells as indicated by the cell quantification analysis (Fig. S12B). The same was observed for the ganglion cell marker RBPMS (Fig. S5). Interestingly, horizontal cells detected by the marker protein Prox1 were found more towards the apical side of organoids while amacrine cells (Ap2α-labelled) were located more towards the centre of organoids (Fig. 5 and Fig. S11), reflecting correct positions of both cell-types within the retinal organization. In all conditions, Müller glia cells (indicated by the CRALBP staining) were observed to span the whole retinal structure akin to what is observed in adult retina (Fig. 5 and Fig. S11). The development of other retinal cell types such as amacrine cells and Müller cells (indicated by the formation of neurofilaments) was also confirmed by TEM (Fig. 3B). In addition, TEM analysis revealed synaptic contacts between retinal cells in all conditions (Fig. 3, arrowheads). Ki67-positive cells (Fig. S9) were

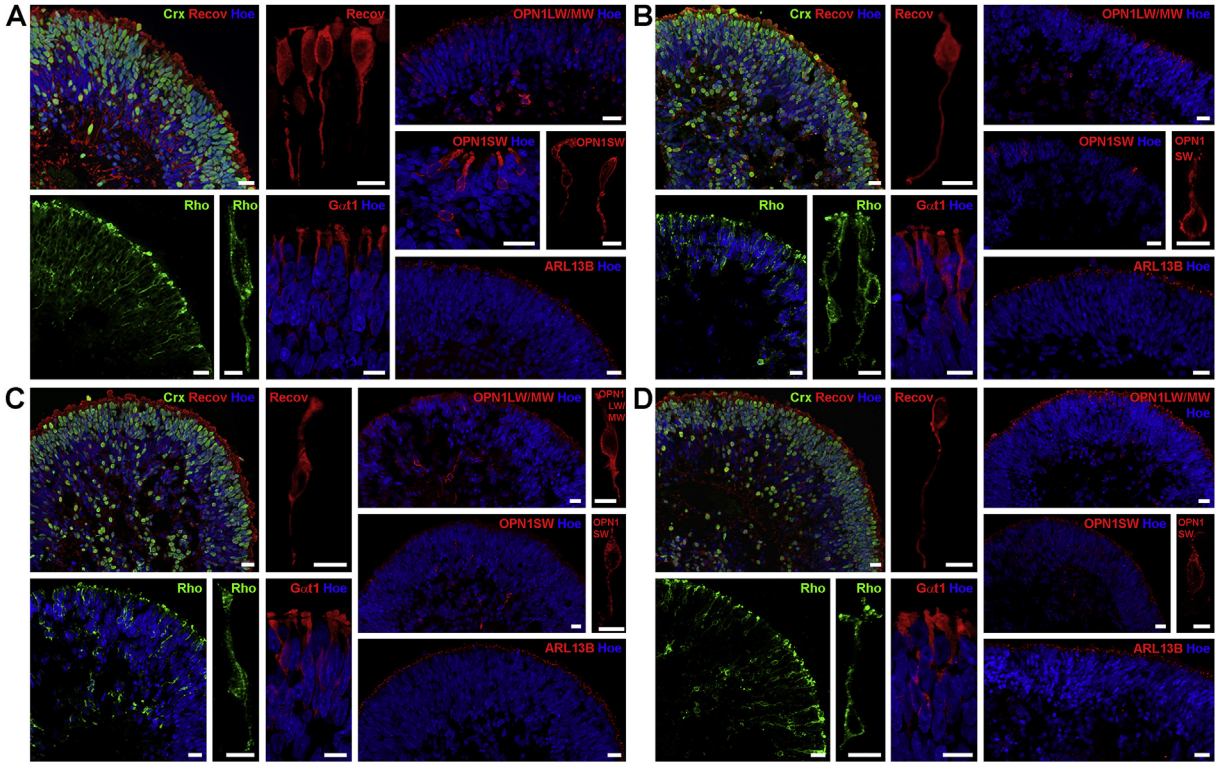

Fig. 4. Photoreceptor characterisation in hESCs-derived retinal organoid at day 150 of differentiation in all culture conditions. (A–D) Expression of photoreceptors (Crx, green; Recoverin, red) including mature marker for rods (Rho, green) and cones (OPN1LW/MW, red; OPN1SW, red) as well as a photoreceptor outer segment (Gαt1, red) and connecting cilium (ARL13B, red) marker in control (A), CM RPE (B), decel NR (C) and decel RPE (D) condition. In all conditions, photoreceptors (rods and cones) displayed the characteristic morphological features of photoreceptors, including the connecting cilium and outer segment formation. Nuclei are counterstained with Hoechst. Abbreviations: Hoe, Hoechst; Rho, Rhodopsin; Recov, Recoverin. Scale bars = 20 μm or 10 μm. (For interpretation of the references to color in this figure legend, the reader is referred to the Web version of this article.)

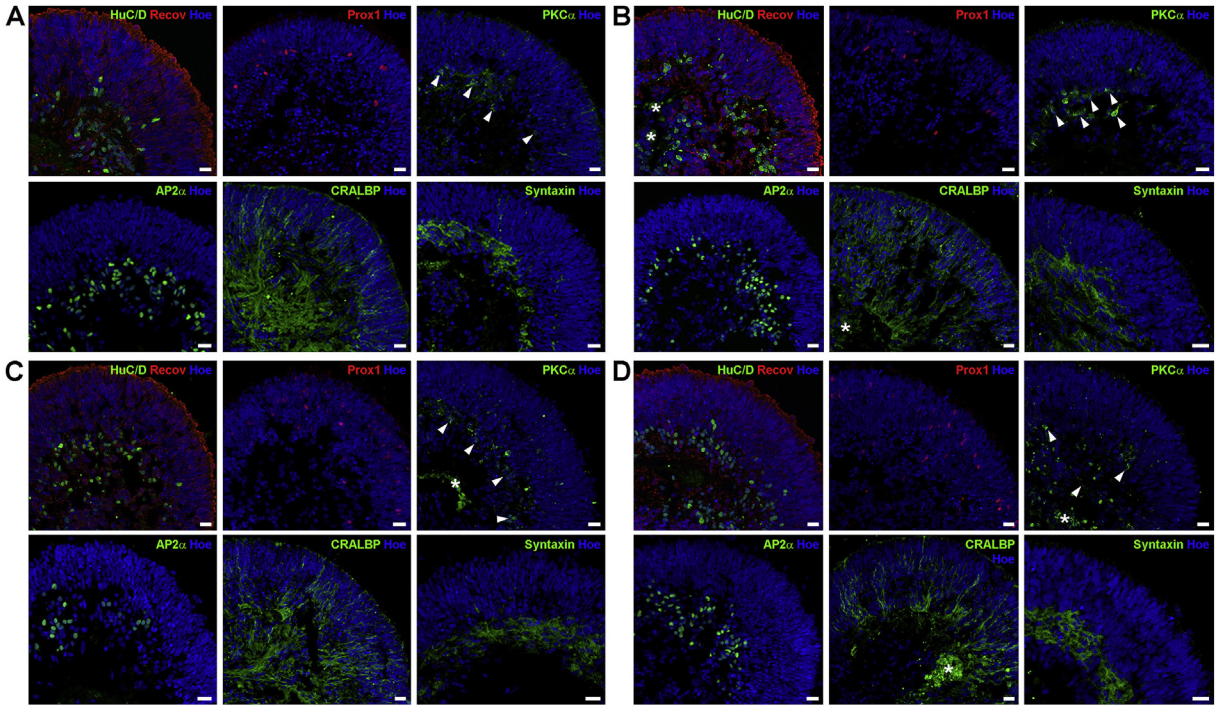

Fig. 5. Retinal cell-type characterisation in hESCs-derived retinal organoid at day 150 of differentiation in all culture conditions. (A–D) Expression of amacrine/ganglion cells (HuC/D, green), bipolar cells (PKCα, green), horizontal cells (Prox1, red), amacrine cells (AP2α, green), Müller cells (CRALBP, green) and synaptic marker (Syntaxin, green) in control (A), CM RPE (B), decel NR (C) and decel RPE (D) condition. All retinal cell-types were expressed in organoids of all four conditions as well as the synaptic marker protein Syntaxin, indicating the formation of synapses between retinal cell types. Nuclei are counterstained with Hoechst. Abbreviations: Hoe, Hoechst. Arrowheads indicate PKCα expression and stars indicate background staining. Scale bars = 20 μm. (For interpretation of the references to color in this figure legend, the reader is referred to the Web version of this article.)

found throughout retinal organoids whereas apoptotic Caspase 3-positive (Fig. S10) cells were seen sporadically at day 150 of differentiation; no significant difference in their abundance was observed between the different culture conditions. Collectively these results suggest that the supplementation of culture media with decel RPE had a positive impact on the development of RPE and rods, whereas the development of other retinal cell types including cones was not affected by the supplementation of CM RPE, decel NR or decel RPE at the later stages of differentiation.

3.4. Effect of ECM supplementation on synaptogenesis and the emergence of light responses

We demonstrated that retinal organoids derived from pluripotent stem cells in all conditions contained all retinal cell-types within a laminated structure similar to the adult retina. But the formation of correct synaptic connections between different cell-types within specialised plexiform layers (outer and inner plexiform layers (OPL and IPL respectively)) as in the normal developing retina, is still challenging for most retinal differentiation protocols [54]. Using synaptic and ribbon synapse specific marker proteins, IHC was performed to investigate the effect of different ECM supplementation at day 150 of differentiation.

Syntaxin, a marker for the presynaptic plasma membrane, was found underneath the putative ONL of retinal organoids in all conditions at day 150 of differentiation (Fig. 5 and Fig. S11), indicating the formation of putative photoreceptor synapses. IHC analysis with ribbon synapse marker proteins (Bassoon and CtBP2) in combination with vGlut1 (a marker for synaptic terminals of photoreceptors and bipolar cells) and Recoverin was carried out to assess this in more detail. Bassoon and CtBP2 immunoreactivity patches were largely found below photoreceptor nuclei in retinal organoids derived from both cell lines in all conditions (Fig. 6A and B and Fig. S13A and B). Co-localisation of Bassoon or CtBP2 respectively with vGlut1 and Recoverin was observed at putative axons/axon terminals as highlighted by higher magnification micrographs (Fig. 6A, B and Fig. S13A and B). This suggests that photoreceptors form synaptic connections with second order neurons (bipolar or horizontal cells).

In addition, quantification of Bassoon and CtBP2 patches as well as their median intensity was performed to validate the impact of different ECM supplementation on synaptogenesis. The number of Bassoon-positive patches was significantly smaller in the CM RPE condition compared to control condition (Fig. 6C), suggesting that the formation of synapses between photoreceptors and second order neurons was less likely to occur in this condition at day 150 of differentiation. In contrast, immunoreactive-positive patches for CtBP2 were not affected by supplementation of culture media with different ECM components (Fig. 6D). Bassoon and CtBP2 protein expression, analysed by the median intensity quantification, revealed a significant increase in all ECM supplemented conditions compared to control (Fig. 6E and F), indicating that culturing organoids with different ECM supplementations promotes the expression of proteins that are essential for synaptic transmission between photoreceptors and their postsynaptic partners. In this context, it is important to note the presence of RIMS1 (Regulating Synaptic Membrane Exocytosis 1) and/or RIMS2 (Regulating Synaptic Membrane Exocytosis 2) peptides in the decel RPE and decel NR samples (Table S5, Table S4).

To functionally validate the formation of these synaptic connections, we performed multielectrode array (MEA) recordings from the putative GCL to investigate how these cells respond to strong white light pulse (WLP) stimuli. Many presumed ON RGCs in retinal organoids derived from hESCs and hiPSCs in control, CM RPE, decel NR and decel RPE conditions at day 150 of differentiation exhibited increase in spiking activity when exposed to high intensity WLP stimuli. The spike raster plots illustrated in Fig. 7A–D shows all ON responses for RGCS that responded at least with a 25% increase in spiking activity following WLP. Panel E illustrates the normalised mean change in spiking activity

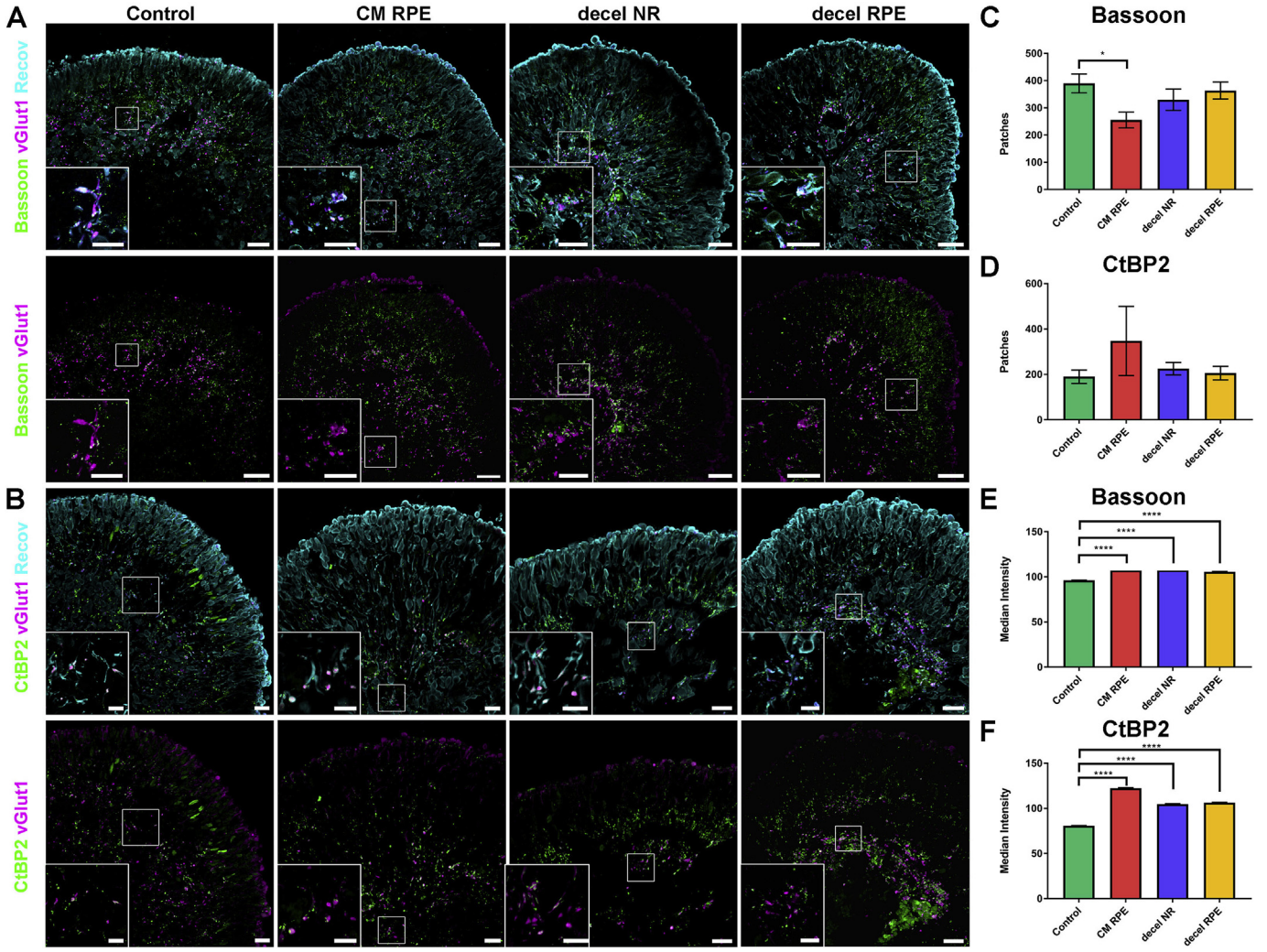

Fig. 6. Synaptic marker expression in hESCs-derived retinal organoids at day 150 in all culture conditions.(A, B) Expression of synaptic marker Bassoon (green; A) and CtBP2 (green; B) in combination with Recoverin (Recov, cyan) and vGlut1 (magenta) in control, CM RPE, decel NR and decel RPE condition of retinal organoids derived from hESCs. Co-localisation of all marker (A,B insets in top panels) and Bassoon (A, bottom panels) or CtBP2 (B, bottom panels) in combination with vGlut1 indicates putative photoreceptor synapses at axon terminals. Abbreviations: Recov, Recoverin. Scale bars = 20 μm or 10 μm (insets). (C, D) Quantification of Bassoon- (C) and CtBP2- (D) immunoreactive patches in hPSCs-derived organoids showed a significant decrease of Bassoon patches in CM RPE condition compared to control. (E, F) Median intensity quantification of Bassoon (E) and CtBP2 (F) in hPSCs-derived retinal organoids revealed an increase of CM RPE, decel NR and decel RPE when compared to control condition. Data is shown as mean ± SEM, n = 6–8 experiments performed in hESCs and hiPSCs. Differences were considered statistically significant at *$p < 0.05$ and ****$p < 0.0001$. (For interpretation of the references to color in this figure legend, the reader is referred to the Web version of this article.)

for all conditions, demonstrating a global increase in responsiveness in all conditions compared to their respective controls. However, the only conditions showing statistically significant increases were the decel NR and decel RPE (Fig. 7E). In summary, these results showed that both decel NR and RPE ECM supplemented conditions improved the light-driven responses compared with the control.

4. Discussion

To date there has been immense progress in generation of organoids from primary and neoplastic tissues and pluripotent stem cells. Retinal organoids in particular have attracted a lot of excitement and interest in view of their intrinsic self-organisation into lamina (layers) which resemble the adult human retina [55] and the presence of all key retinal cell types. The ability to generate large amount of retinal cells for cell based therapies and to provide a test bed for drug testing and pharmacology screens, makes the pluripotent stem cell retinal organoids the most optimal tool to date. Notwithstanding this fast progress, current differentiation protocols are impeded by several key challenges which include the inability generate the correct proportions of all retinal cell types and to maintain the three clearly separated nuclear layers in long term cultures, failure to establish correct synaptic connections and inability to elicit light responses which are fully comparable to adult retina [40]. Published evidence shows that the early stages of retinal differentiation (eyefield formation, emergence of optic vesicles and optic cups) is influenced by the activity of key developmental pathways including WNT/FGF/TGFβ/BMP etc. [56]); however photoreceptor survival, emergence and maturation is critically dependent on the interaction with closely situated RPE cells and other retinal cells [57]. In this context, we hypothesised that adult retina and RPE extracellular matrix and growth factors bound therein, may help to expedite and enhance differentiation, synaptogenesis and light responsiveness of retinal organoids. In the last few years, decellularised ECM has gained a lot of traction in the field of tissue engineering due to their ease of standardised production, constant availability and preservation of key growth factors and ECM components that are essential for guiding stem

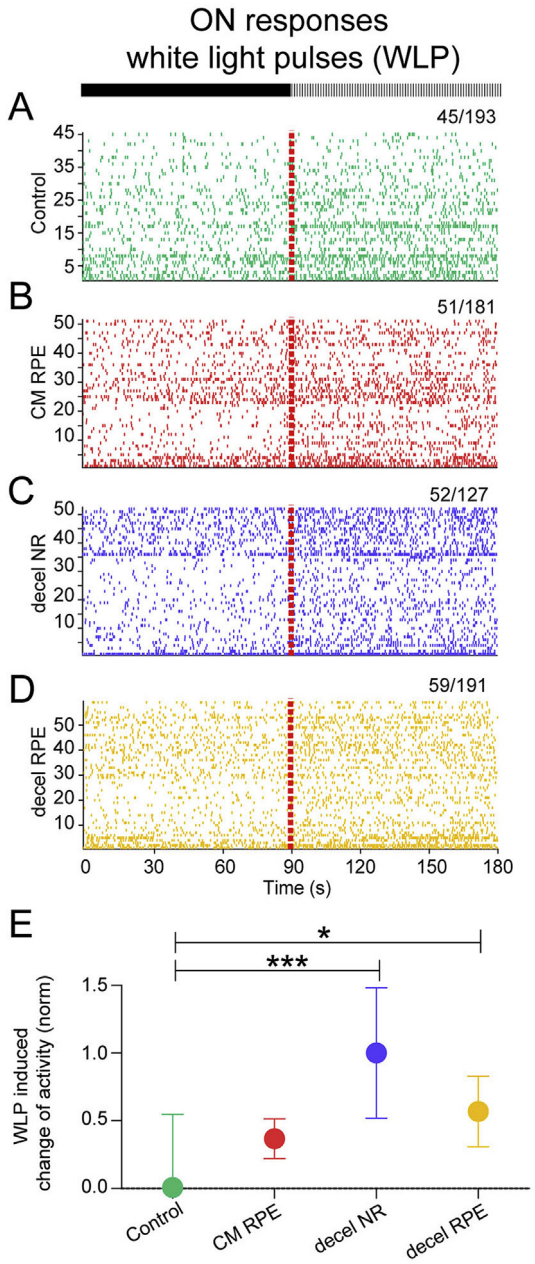

Fig. 7. Light-driven spiking activity recorded from presumed ON RGCs & change of RGC spiking activity in four conditions of retinal organoids derived from hPSCs at day 150 of differentiation. (A–D) Spike raster plots (SRPs) from RGCs of the different groups that showed a 25% increase in spiking activity during pulsed white light (WLP, see methods). In the raster plot, each small vertical bar indicates the time stamp of a spike, where each row represents a different RGC. The left half illustrates the activity before stimulus onset and, separated by the red line, the right half the activity when exposed to WLP. A) SRPs from the control group; B) SRPs from the CM RPE group; C) SRPs from the decel NR group; D) SRPs from the decel RPE group. E) The change of activity before and after stimulus onset was calculated for each RGC shown in A-D. An unpaired t-test was applied this data to estimate the difference between the control group to the other three groups, differences were considered statistically significant for (E) decel RPE vs control *p = 0.0148 and decel NR vs control ***p = 0.0009. For better visualisation the means (+SEM) were normalised (as a fraction) within each cell line. (For interpretation of the references to color in this figure legend, the reader is referred to the Web version of this article.)

cell differentiation. Although decellularised ECM generation from bovine neural retina has been reported [36], its application as a media supplement in pluripotent stem cell differentiation to 3D retinal organoids has not been carried out previously. In this manuscript we report the successful preparation of decel ECM-derived peptide mixes from bovine NR and RPE and their characterisation by quantitative proteomic analysis and we show that retinal specific decellularised retinal matrices retain essential peptides belonging to well described ECM components (e.g. collagen, laminin, versican), albeit some of these were decreased during the decellularisation process. Addition of these decellularised ECM-derived peptide mixes to the culture media did not seem to affect the early- or mid-stages of differentiation, but it did enhance rod photoreceptor emergence, expression of synaptic markers and light responsiveness of retinal organoids generated from hESCs and hiPSCs, providing for the first time evidence that retinal niches (RPE and NR) contain ECM-peptides and/or growth factors which are useful for generation and function of retinal organoids. We performed quantitative mass spectrometry of the peptide mixes derived from decellularisation of NR and RPE and showed differential abundance of collagen chains and versican between the two peptide mixes, which may underline some of the differences in phenotypic consequences reported from this study. However, more targeted studies using supplementation with these differentially expressed ECM peptides are needed to further optimise retinal organoid differentiation from human pluripotent stem cells and their functionality.

It is now well established that RPE plays a critical role in the maintenance of photoreceptors and that RPE cell death and dysfunction is an important cause of many retinal dystrophies. Genetic ablation of RPE in animal models has been shown to lead to a rapid and profound reduction in RPE cell number [58] and a significant reduction in scotopic amplitude of the electroretinogram and a wave gradient. Together these published findings suggest that the functionality and survival of the rod photoreceptors is critically dependent on the RPE cells. This is also corroborated by our study for the addition of decel RPE or CM RPE enhanced rod generation at the later stages of retinal differentiation (day 150). A significant increase in rhodopsin expression was also noted, corroborating data reported by German et al. showing that RPE cells promote the synthesis of rhodopsin from photoreceptors under *in vitro* conditions [16]. This effect is cell type specific, as the development of other retinal cells (cones, bipolar, horizontal, amacrine, ganglion and Müller cells) was not affected by the various ECM supplementations.

The generation of retinal organoids containing key retinal cell types from hESCs and hiPSCs have now been reported in several studies [1–6]. However, the formation of correct synaptic connections between different cell-types remains a challenge in the field of retinal differentiation, albeit the expression of synaptic markers has been observed [54]. The retinal organoids in this study were able to generate synaptic connections between photoreceptors and second order neurons such as bipolar or horizontal cells. Our analysis showed that all three media supplementations indicated increased the expression of the synaptic markers, Bassoon and CtBP2, compared to the control conditions. Recently, our group has reported that light responses obtained from hESCs and hiPSCs derived retinal organoids are rather immature and comparable to the earliest light responses recorded from the neonatal mouse retina, close to the period of eye opening [59]. To assess whether ECM supplementation had any impact on retinal function, electrophysiological light responses were performed, which showed that decel NR and RPE supplementation significantly enhanced the light responsiveness of retinal organoids [59]. Despite the demonstrated enhancement of retinal organoid light sensitivity, the light-driven responses are still very immature and not yet comparable to responses from a fully developed adult retina. The ontogeny of light-driven RGC responses depend on molecular cues and activity-dependent refinement (for review, see Ref. [60]). The refinement of synapses onto RGCs and amacrine cells (AC) continues after eye-opening and depends upon visual experience [61,62]. The light responses presented in this study are

weak and sluggish, comparable to responses recorded shortly before eye-opening in the developing mouse retina [59]. Although the photoreceptor synapses seem to reach a reasonable level of maturity in all conditions, it is very likely that the bipolar synapses in the outer and inner plexiform layer are not fully mature yet. The ECM supplemented conditions enhanced the light-driven ON RGC responses. These are indeed very promising findings, although it remains to be determined whether such effect is due to enhanced expression of important building blocks of synaptic functionality and/or the higher number of rods and RPE cells found in retinal organoids cultured in the presence of decel RPE [59].

In summary, out data indicate that decellularised ECM-derived peptides generated from neural retina and RPE play an important role in photoreceptor maturation, synaptogenesis and light responsiveness of pluripotent stem cell derived retinal organoids. The decellularised ECM-derived peptides are easy to generate, amenable to scale up and 3D culture conditions, opening up new possibilities for generation of retinal organoids which mimic adult human retina both in cell type composition and function. Further studies are however needed to assess the immunogenic profile of decellularised ECM matrices in animal models before proceeding with pre-clinical studies.

Author contributions

BD: experimental design and execution, data analysis; manuscript and figure preparation;

MF: experimental design and execution, data analysis; manuscript and figure preparation;

GH: experimental design and execution, data analysis; figure and manuscript preparation;

MK, DZ, NCH, MD, PW, DH, KWYD: experimental execution, figure preparation, data analysis;

NK, JAA, HZH, ES: experimental execution, data analysis, fund raising.

ML: study design, data analysis, manuscript and figure preparation and fund raising.

All authors approved the final version of the manuscript.

Acknowledgments

This work was funded by the ERC Consolidator award (grant number #614620), the RPFB Innovation award (grant number #GR584), MRC Confidence in Concept award (MC_PC_15030), MRC “MICA: The Newcastle Proximity Laboratory” (MR/N005872/1, Deanship of Scientific Research (DSR) of King Abdul Aziz University, Jeddah (grant number 1-287-1434-HiCi), MRC Confidence in Concept award (MC_PC_15030). The authors are grateful to Lisa Hodgson for help with the microscopy and members of Lako's group for fruitful discussions.

Appendix A. Supplementary data

Supplementary data to this article can be found online at https://doi.org/10.1016/j.biomaterials.2019.01.028.

References

[1] M. Eiraku, et al., Self-organizing optic-cup morphogenesis in three-dimensional culture, Nature 472 (7341) (2011) 51–U73.
[2] M. Eiraku, Y. Sasai, Mouse embryonic stem cell culture for generation of three-dimensional retinal and cortical tissues, Nat. Protoc. 7 (1) (2011) 69–79.
[3] T. Nakano, et al., Self-formation of optic cups and storable stratified neural retina from human ESCs, Cell Stem Cell 10 (6) (2012) 771–785.
[4] J. Assawachananont, et al., Transplantation of embryonic and induced pluripotent stem cell-derived 3D retinal sheets into retinal degenerative mice, Stem Cell Reports 2 (5) (2014) 662–674.
[5] A. Kuwahara, et al., Generation of a ciliary margin-like stem cell niche from self-organizing human retinal tissue, Nat. Commun. 6 (2015) 6286.
[6] N. Takata, et al., An eye organoid approach identifies Six3 suppression of R-spondin 2 as a critical step in mouse neuroretina differentiation, Cell Rep. 21 (6) (2017) 1534–1549.
[7] A. Gonzalez-Cordero, et al., Photoreceptor precursors derived from three-dimensional embryonic stem cell cultures integrate and mature within adult degenerate retina, Nat. Biotechnol. 31 (8) (2013) 741–747.
[8] M. Völkner, et al., Retinal organoids from pluripotent stem cells efficiently recapitulate retinogenesis, Stem Cell Reports 6 (4) (2016) 525–538.
[9] X. Zhong, et al., Generation of three-dimensional retinal tissue with functional photoreceptors from human iPSCs, Nat. Commun. 5 (2014) 4047.
[10] J.S. Meyer, et al., Optic vesicle-like structures derived from human pluripotent stem cells facilitate a customized approach to retinal disease treatment, Stem Cell. 29 (8) (2011) 1206–1218.
[11] A. Gonzalez-Cordero, et al., Recapitulation of human retinal development from human pluripotent stem cells generates transplantable populations of cone photoreceptors, Stem Cell Reports 9 (3) (2017) 820–837.
[12] K.J. Wahlin, et al., Photoreceptor outer segment-like structures in long-term 3D retinas from human pluripotent stem cells, Sci. Rep. 7 (1) (2017) 766.
[13] R. Kaewkhaw, et al., Transcriptome Dynamics of developing photoreceptors in three-dimensional retina cultures recapitulates temporal sequence of human cone and rod differentiation revealing cell surface markers and gene networks, Stem Cell. 33 (12) (2015) 3504–3518.
[14] A. Lowe, et al., Intercellular adhesion-dependent cell survival and ROCK-regulated actomyosin-driven forces mediate self-formation of a retinal organoid, Stem Cell Reports 6 (5) (2016) 743–756.
[15] S.M. Raymond, I.J. Jackson, The retinal pigmented epithelium is required for development and maintenance of the mouse neural retina, Curr. Biol. 5 (11) (1995) 1286–1295.
[16] O.L. German, et al., Retinal pigment epithelial cells promote spatial reorganization and differentiation of retina photoreceptors, J. Neurosci. Res. 86 (16) (2008) 3503–3514.
[17] S. Aisenbrey, et al., Retinal pigment epithelial cells synthesize laminins, including laminin 5, and adhere to them through alpha3- and alpha6-containing integrins, Invest. Ophthalmol. Vis. Sci. 47 (12) (2006) 5537–5544.
[18] S.J. Clark, et al., Mapping the differential distribution of glycosaminoglycans in the adult human retina, choroid, and sclera, Invest. Ophthalmol. Vis. Sci. 52 (9) (2011) 6511–6521.
[19] T.D. Keenan, et al., Mapping the differential distribution of proteoglycan core proteins in the adult human retina, choroid, and sclera, Invest. Ophthalmol. Vis. Sci. 53 (12) (2012) 7528–7538.
[20] A.M. Kolomeyer, I.K. Sugino, M.A. Zarbin, Characterization of conditioned media collected from cultured adult versus fetal retinal pigment epithelial cells, Invest. Ophthalmol. Vis. Sci. 52 (8) (2011) 5973–5986.
[21] V.P. Gaur, Y. Liu, J.E. Turner, RPE conditioned medium stimulates photoreceptor cell survival, neurite outgrowth and differentiation in vitro, Exp. Eye Res. 54 (5) (1992) 645–659.
[22] J. Hsiung, et al., Retinal pigment epithelial cell conditioned medium enhances the yield of RPE cells differentiated from human embryonic stem cells, J. Clin. Exp. Pathol. 5 (2) (2015) 216.
[23] A.M. Kolomeyer, I.K. Sugino, M.A. Zarbin, Characterization of the effects of retinal pigment epithelium-conditioned media on porcine and aged human retina, Graefes Arch. Clin. Exp. Ophthalmol. 251 (6) (2013) 1515–1528.
[24] S. Kaempf, et al., Novel organotypic culture model of adult mammalian neurosensory retina in co-culture with retinal pigment epithelium, J. Neurosci. Methods 173 (1) (2008) 47–58.
[25] K.R. Chirco, et al., Preparation and evaluation of human choroid extracellular matrix scaffolds for the study of cell replacement strategies, Acta Biomater. 57 (2017) 293–303.
[26] H.C. Ott, et al., Perfusion-decellularized matrix: using nature's platform to engineer a bioartificial heart, Nat. Med. 14 (2) (2008) 213–221.
[27] D. Sun, et al., Novel decellularized liver matrix-alginate hybrid gel beads for the 3D culture of hepatocellular carcinoma cells, Int. J. Biol. Macromol. 109 (2018) 1154–1163.
[28] P.M. Baptista, et al., The use of whole organ decellularization for the generation of a vascularized liver organoid, Hepatology 53 (2) (2011) 604–617.
[29] T.H. Petersen, et al., Tissue-engineered lungs for in vivo implantation, Science 329 (5991) (2010) 538–541.
[30] H.C. Ott, et al., Regeneration and orthotopic transplantation of a bioartificial lung, Nat. Med. 16 (8) (2010) 927–933.
[31] J.J. Song, et al., Regeneration and experimental orthotopic transplantation of a bioengineered kidney, Nat. Med. 19 (5) (2013) 646–651.
[32] J. De Waele, et al., 3D culture of murine neural stem cells on decellularized mouse brain sections, Biomaterials 41 (2015) 122–131.
[33] G. Agmon, K.L. Christman, Controlling stem cell behavior with decellularized extracellular matrix scaffolds, Curr. Opin. Solid State Mater. Sci. 20 (4) (2016) 193–201.
[34] X. Zhang, J. Dong, Direct comparison of different coating matrix on the hepatic differentiation from adipose-derived stem cells, Biochem. Biophys. Res. Commun. 456 (4) (2015) 938–944.
[35] S. Ponce Márquez, et al., Decellularization of bovine corneas for tissue engineering applications, Acta Biomater. 5 (6) (2009) 1839–1847.
[36] J. Kundu, et al., Decellularized retinal matrix: natural platforms for human retinal progenitor cell culture, Acta Biomater. 31 (2016) 61–70.
[37] J. Ji, et al., Decellularized matrix of adipose-derived mesenchymal stromal cells enhanced retinal progenitor cell proliferation via the Akt/Erk pathway and neuronal differentiation, Cytotherapy 20 (1) (2018) 74–86.

[38] D. Singh, et al., A biodegradable scaffold enhances differentiation of embryonic stem cells into a thick sheet of retinal cells, Biomaterials 154 (2018) 158–168.
[39] T.H. Tezel, L.V. Del Priore, H.J. Kaplan, Reengineering of aged Bruch's membrane to enhance retinal pigment epithelium repopulation, Invest. Ophthalmol. Vis. Sci. 45 (9) (2004) 3337–3348.
[40] D. Hallam, et al., An induced pluripotent stem cell patient specific model of complement factor H (Y402H) polymorphism displays characteristic features of age-related macular degeneration and indicates a beneficial role for UV light exposure, Stem Cell. 35 (11) (2017) 2305–2320.
[41] A. Buskin, et al., Disrupted alternative splicing for genes implicated in splicing and ciliogenesis causes PRPF31 retinitis pigmentosa, Nat. Commun. 9 (1) (2018) 4234.
[42] C.J. Medberry, et al., Hydrogels derived from central nervous system extracellular matrix, Biomaterials 34 (4) (2013) 1033–1040.
[43] N. Di Ferrante, Turbidimetric measurement of acid mucopolysaccharides and hyaluronidase activity, J. Biol. Chem. 220 (1) (1956) 303–306.
[44] R. Rago, J. Mitchen, G. Wilding, DNA fluorometric assay in 96-well tissue culture plates using Hoechst 33258 after cell lysis by freezing in distilled water, Anal. Biochem. 191 (1) (1990) 31–34.
[45] D. Melguizo-Sanchis, et al., iPSC modeling of severe aplastic anemia reveals impaired differentiation and telomere shortening in blood progenitors, Cell Death Dis. 9 (2) (2018) 128.
[46] C.B. Mellough, et al., IGF-1 signaling plays an important role in the formation of three-dimensional laminated neural retina and other ocular structures from human embryonic stem cells, Stem Cell. (2015).
[47] M. Felemban, et al., Extracellular matrix component expression in human pluripotent stem cell-derived retinal organoids recapitulates retinogenesis in vivo and reveals an important role for IMPG1 and CD44 in the development of photoreceptors and interphotoreceptor matrix, Acta Biomater. 74 (2018) 207–221.
[48] C. Zimmer, et al., Segmentation and tracking of migrating cells in videomicroscopy with parametric active contours: a tool for cell-based drug testing, IEEE Trans. Med. Imag. 21 (10) (2002) 1212–1221.
[49] J.N. Kapur, P.K. Sahoo, A.K.C. Wong, A new method for gray-level picture thresholding using the entropy of the histogram, Comput. Vis. Graph Image Process 29 (3) (1985) 273–285.
[50] G. Hilgen, et al., Pan-retinal characterisation of light responses from ganglion cells in the developing mouse retina, Sci. Rep. 7 (2017) 42330.
[51] J.O. Muthmann, et al., Spike detection for large neural populations using high density multielectrode arrays, Front. Neuroinf. 9 (2015) 28.
[52] G. Hilgen, et al., Unsupervised spike sorting for large-scale, high-density multielectrode arrays, Cell Rep. 18 (10) (2017) 2521–2532.
[53] B. Dorgau, et al., Laminin γ3 plays an important role in retinal lamination, photoreceptor organisation and ganglion cell differentiation, Cell Death Dis. 9 (6) (2018) 615.
[54] S. Llonch, M. Carido, M. Ader, Organoid technology for retinal repair, Dev. Biol. 433 (2) (2018) 132–143.
[55] N.C. Hunt, et al., The application of biomaterials to tissue engineering neural retina and retinal pigment epithelium, Adv. Healthc. Mater. (2018) e1800226.
[56] C.B. Mellough, et al., Lab generated retina: realizing the dream, Vis. Neurosci. 31 (4–5) (2014) 317–332.
[57] J.A. Brzezinski, T.A. Reh, Photoreceptor cell fate specification in vertebrates, Development 142 (19) (2015) 3263–3273.
[58] R. Longbottom, et al., Genetic ablation of retinal pigment epithelial cells reveals the adaptive response of the epithelium and impact on photoreceptors, Proc. Natl. Acad. Sci. Unit. States Am. 106 (44) (2009) 18728–18733.
[59] D. Hallam, et al., Human induced pluripotent stem cells generate light responsive retinal organoids with variable and nutrient dependent efficiency, Stem Cell. (2018).
[60] N. Tian, Developmental mechanisms that regulate retinal ganglion cell dendritic morphology, Dev Neurobiol 71 (12) (2011) 1297–1309.
[61] N. Tian, Visual experience and maturation of retinal synaptic pathways, Vis. Res. 44 (28) (2004) 3307–3316.
[62] Q. He, P. Wang, N. Tian, Light-evoked synaptic activity of retinal ganglion and amacrine cells is regulated in developing mouse retina, Eur. J. Neurosci. 33 (1) (2011) 36–48.